Available online at www.eccomasproceedia.org
Eccomas Proceedia COMPDYN (2023) 511-527

ECCOMAS
Proceedia

COMPDYN 2023
9th ECCOMAS Thematic Conference on
Computational Methods in Structural Dynamics and Earthquake Engineering
M. Papadrakakis, M. Fragiadakis (eds.)
Athens, Greece, 12-14 June 2023

SHAKING TABLE TESTS ON SCALED TWO-FLOOR STEEL FRAMED STRUCTURES – DESIGN AND PRELIMINARY NUMERICAL INVESTIGATIONS

G. Balaskas[1], C. Vulcu[1], B. Hoffmeister[1] and C. Butenweg[1]

[1] Center for Wind and Earthquake Engineering, RWTH-Aachen University

Mies-van-der-Rohe-Str. 1, Aachen, Germany
e-mail: {g.balaskas, c.vulcu, hoff}@stb.rwth-aachen.de, butenweg@lbb.rwth-aachen.de

Abstract

Structural Health Monitoring (SHM) can allow for rapid structural damage detection in the aftermath of an earthquake event. Especially, regarding industrial facilities depending on the seismic performance of critical components, automated counter measures could be activated to prevent domino effects and lead to damage mitigation. Real-time seismic damage detection through SHM is a promising, but challenging field. Although various methods, regarding structural damage detection, have been developed the previous years, a holistic approach is still missing. In the framework of an ongoing German nationally funded research project, an interdisciplinary, user-oriented earthquake early warning and rapid response system was developed. Part of the project were shaking table tests on steel space framed test structure. The objective of the investigation was to: (i) validate damage sensitive indicators, arranged based on numerical simulations and literature; (ii) investigate the effectiveness of measuring and identification methods; and (iii) correlate the measured data with the performance of the structure. Output-only and input-output methods in time and frequency domain will be used for the damage detection scheme. Three configurations of steel moment resisting frames (MRF) with different beam-to-column joints are currently being tested. This paper summarizes the preliminary numerical investigations for the design of the test structure. Beam-to-column and column base joints were analyzed using advanced finite element numerical simulations and their properties were implemented in global structural models. Response history analyses were used as a prognosis for the ongoing experimental tests. The instrumentation concept and the experimental program are also outlined in this contribution.

Keywords: Shaking Table Tests, Damage Detection, Steel Structures, Seismic Risk in Industrial Facilities, Earthquake Early Warning and Rapid Response System.

ISSN:2623-3347
Peer-review under responsibility of the organizing committee of COMPDYN 2023.
doi: 10.7712/120123.10417.20759

1 INTRODUCTION

Within the research project "ROBUST", an early warning and rapid response system based on a network of interconnected smart seismic and structural health monitoring sensors distributed in Lower Rhine Region was developed [1]. Main objective of the project was to provide useful information to facility managers and public authorities about the seismic performance of critical infrastructures in almost real time. On the one hand, the seismic sensor network through a communication platform forwards warning messages about an upcoming seismic event and an estimation of its magnitude - approximately a few seconds (depending on the epicenter of the earthquake) before it reaches critical infrastructures. On the other hand, SHM systems permanently installed on critical infrastructures using an ensemble of Damage Sensitive Indicators (DSI) can assess the seismic performance of the monitored structures right after the seismic event. The structural health status of those infrastructures will be sent to the corresponding end-users, who are registered as "subscribers" for each facility of interest within the communication platform. Each subscriber (facility managers, public authorities, rescue teams) has access to different level and detail of information, depending on his role and responsibility (user-oriented system).

Damage detection using SHM usually depends on the identification of changes in vibration properties [2][3]. Swifts on estimators of natural frequencies and changes of mode-shape curvature are used to detect the existence of damage and its location. Measurements prior to the seismic event representing the "healthy" state are compared with the post-earthquake vibration measurements [3][4][5][6][7]. Structure-specific models are needed to quantify the damage and predict the load carrying capacity after the seismic event [8][9][10]. In case of concrete or masonry structures, the presence of cracks after a moderate or strong event affects straight-forward the structure's stiffness and is sensitive to vibration measurements. However, regarding steel MRFs, especially when they are slightly or moderately damaged, the change of the fundamental frequency is rather low [11], which settles the damage identification even more challenging.

The latest years, there is an increasing tendency to complete the traditional vibration-based methods with the use of machine learning (ML) applications [12]. This enables the training of different damage-sensitive indicators as classifiers to indicate the presence, location, and severity of structural damage [13][14]. Within this approach many indicators can be weighted properly, after a training process and result in a multi-parametric identification process. Because of the scarcity of data from monitored buildings that suffered a strong motion event, most of the applications are based on simulated structures, which obviously contain inherent bias. An intermediate solution between simulations and real buildings are shaking-table tests of scaled structures. In the framework of the ROBUST research project, shaking table tests, in a scaled representation of the monitored facility, were designed and are to be carried out in the near future. In the current paper, the experimental program as well as the pre-test numerical analyses are outlined.

2 REAL FACILITY AND TEST STRUCTURE

The industrial facility, which was selected as a case study within the research project ROBUST, comprised many typical structural properties of industrial facilities for the chemical industry. It was realized in a bare steel solution with floors of metal gratings and appropriate openings at the floors for facility-specific process components (combustion chambers, chimney, distillation columns etc.), as illustrated in Figure 2. Furthermore, despite the presence of many secondary beams, no rigid diaphragm at floor level can be considered a priori.

Consequently, stabilizing frames (in this case moment resisting) were built in all main axes. The choice of the structural system, namely MRF, was governed mainly by spatial and technical flexibility, as MRFs allow for future reassembling of the production line and reallocation of pipelines. The reference structure was a two-floor steel frame structure. In longitudinal direction, the structure consisted of three three-bay frames (axes 1-3), whereas in transverse direction of four two-bay frames. In both directions, only one bay in each axis was considered as moment-resisting, see Figure 1 and Figure 2. The moment-resisting joints were realized as equal-strength, semi-rigid, haunched joints. Within the research project, a permanent SHM system will be installed at the selected reference structure.

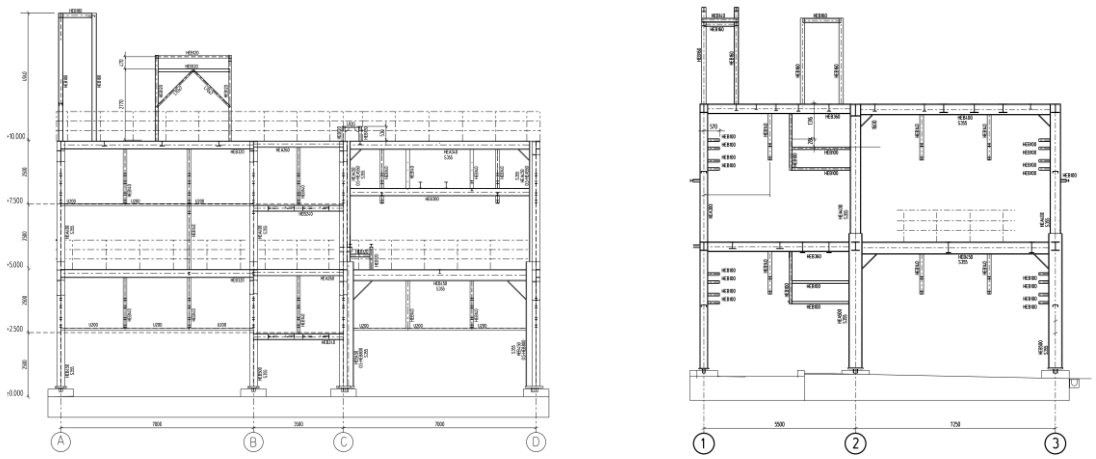

(a) (b)

Figure 1: Monitored chemical facility (a) longitudinal axis 1, (b) transverse axis A.

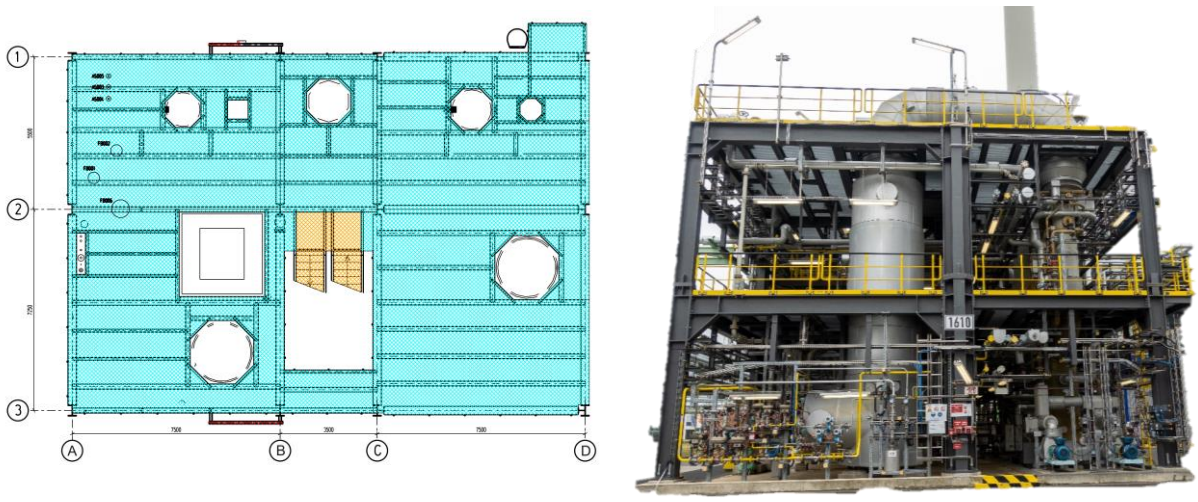

(a) (b)

Figure 2: Monitored chemical facility: (a) floor view (b) view from axis D.

The developed test structure adopted many properties of the reference chemical facility but was also adapted to the boundary conditions of the available shaking test from the Chair of Structural Dynamics, RWTH Aachen University, which can provide dynamic excitation only in one direction. The test structure was a two-floor, one-bay, moment-resisting steel frame. In the excitation direction, the structural system was MRF, whereas in the other direction, the test structure was stabilized by braces. Three different bolted moment resisting beam-to-column joints attached on frame specimens were designed: (i) haunched joint (SP1-HJ), (ii) reduced beam section joint (SP2-RBS) and (iii) extended unstiffened end-plate joint for low-

to-moderate seismic areas (SP3-LSJ). The first two variants were designed according to prEN-1998 [15], whereas the latest one was inspired from an ongoing research project [16][17].

The dimensions of the specimen were: 2.40 m length, 2.40 m width and 3.78 m total height (1st floor 2.00 m; 2nd floor 1.78 m). The column web panels were strengthened with two supplementary web plates (SWP) and six continuity plates (CP) for each moment-resisting joint. To realize the different configurations only the frame girders must be replaced. The properties of the frames and their detailing are illustrated in Figure 3 and Figure 4 and outlined in Table 1. Four steel I-Profiles with self-weight of 1650 kg (16.5 kN) each, were attached on the main structure as masses and were secured by steel U-profiles. An industrial pressure vessel with dead load of 100 kg was also placed on the first floor. During the first part of the experimental campaign, the pressure vessel remained without content. Its seismic behavior with different filling levels will be examined at the next phase of the experimental program and is out-of-scope of this paper.

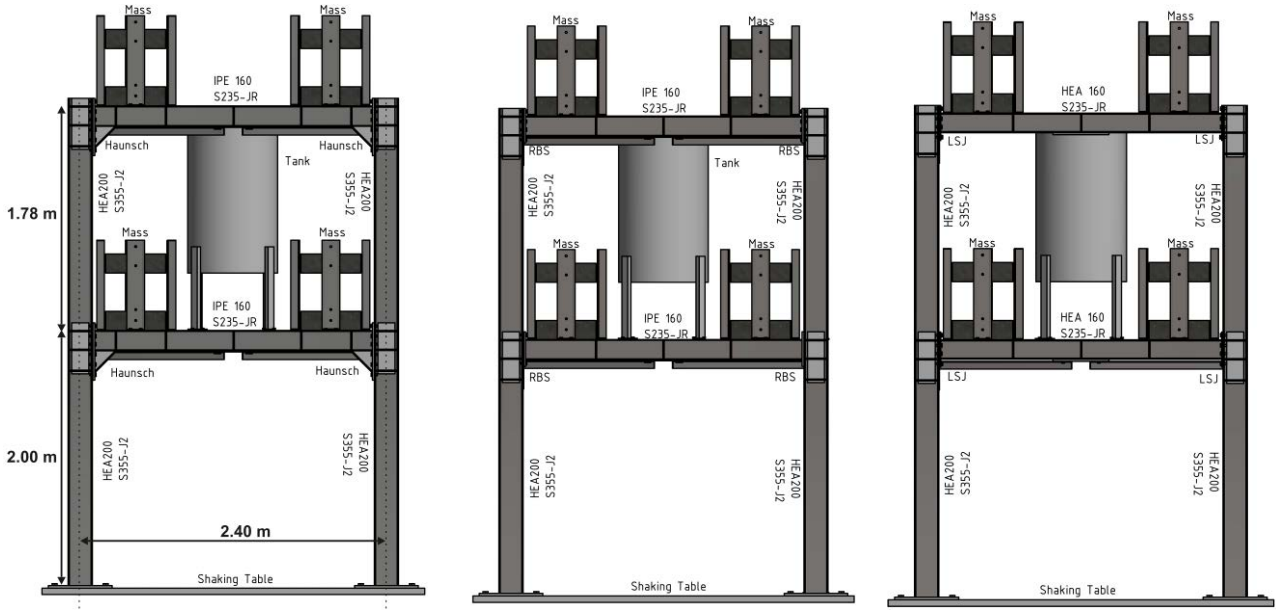

(a) (b) (c)

Figure 3: Experimentally investigated frame configurations; (a) haunched joints (SP1-HJ), (b) reduced beam section joints (SP2-RBS), (c) low seismicity joints (SP3-LSJ).

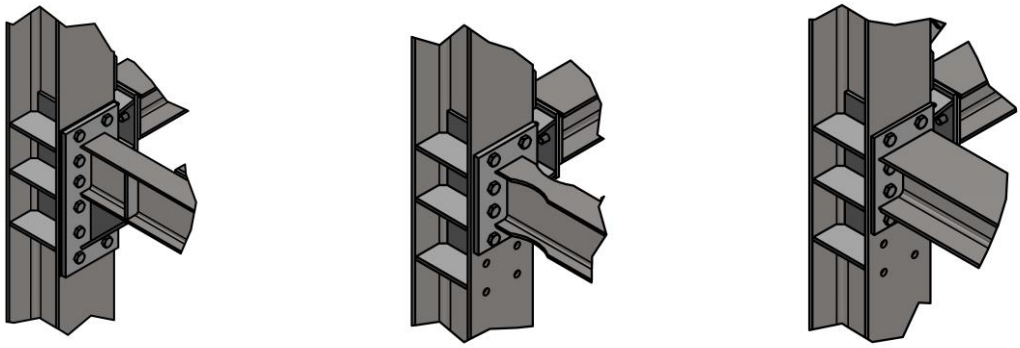

(a) (b) (c)

Figure 4: 3D-Illustration of the MR-joints: (a) haunched joints, (b) reduced beam section joints, (c) low seismicity joints.

The instrumentation system consisted of the global monitoring system, which included all accelerometers and the local monitoring system, which incorporated displacement traducers, inclinometers, and strain gauges. The global monitoring system was connected with the "smart" data acquisition device NI-CompactRio [18], which was responsible for the real-time assessment of data. The global monitoring system will be permanently installed in the industrial facility as SHM system. Three different kinds of accelerometers were used: (i) integrated circuit piezoelectric (ICP) accelerometers, (ii) high resolution – low noise micro electromechanical system (MEMS) accelerometers, (iii) common MEMS accelerometers. Their main properties and their role are summarized in Table 2 while their position is illustrated in Figure 5 & Figure 6. Part of the investigation was to examine the effectiveness of MEMS accelerometers of higher noise level for system identification under low-amplitude ambient excitation compared to more accurate sensors (ICP and MEMS-HR). The local instrumentation scheme was installed mainly on Frame A (Figure 5b) and comprised by: (i) 4 displacement potentiometer with measuring range ±250 mm to record the table and floor horizontal displacements, (ii) 8 displacement traducers with range ±50 mm to measure the local response of the joints, (iii) 2 inclinometers to identify the columns rotation, (iv) 16 uniaxial strain gauges attached to column flanges (CF) (internal and external) to capture the bending moment at both ends of the columns in first and second floor, (v) 2 strain gauges at the bottom of columns A1 and A2 to measure the normal force (tension and compression) at column base and (vi) 14 strain gauges at the dissipative zones, to detect locally the strain concentration.

	SP1-HJ	*SP2-RBS*	*SP3-LSJ*
Columns	HEA200 **S355**-J2 + 2·SWP + 6·CP	HEA200 **S355**-J2 + 2·SWP + 6·CP	HEA200 **S355**-J2 + 2·SWP + 6·CP
Beams	IPE-160 **S235**-JR +2·CP Haunch web: t = 8 mm Haunch flange: t = 8 mm	IPE-160 **S235**-JR RBS Properties acc. [15]: a = 50 mm b = 120 mm c = 20.5 mm	HEA160 **S235**-JR
Bolts	12·M16, 10.9 HV	8·M16, 10.9 HV	8·M16, 10.9 HV
Connection	Full-strength Semi-rigid End-plate (mm): 450·190·15	Full-strength Semi-rigid End-plate (mm): 272·190·15	Partial strength Semi-rigid End-plate (mm): 272·190·8
Welds	Full penetration groove welds	Full penetration groove welds	Full penetration groove welds
Dissipative zone	Beam End	Reduced Beam Section	Connection - End-plate

Table 1: Overview of steel specimens.

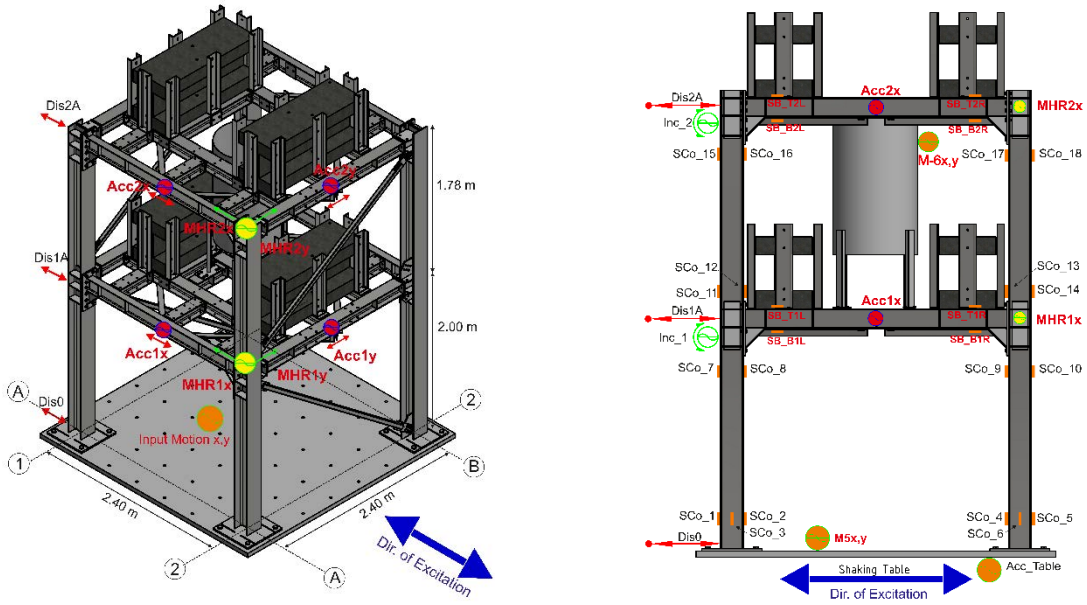

(a) (b)

Figure 5: Instrumentation scheme (a) 3D view of the structure (b) Instrumentation of frame in axis A.

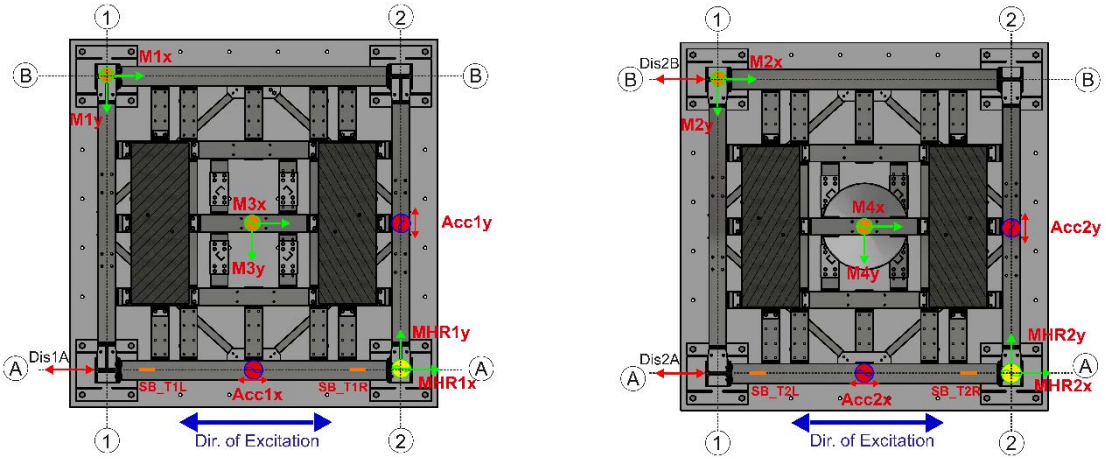

(a) (b)

Figure 6: Instrumentation Scheme – Floor views (a) First floor (b) Second floor.

The local instrumentation of the joints was adapted to the characteristics of each configuration. Target was to define reliable local damage indicators. In each case, strains were measured at top and bottom beam flange at the positions, where plastic deformations were expected (Figure 7). In addition, for the haunched joints, the diagonal relative displacement (see Figure 7a: RD1a) between column and beam was recorded, in order to calculate, given the initial vertical and horizontal distances of the two point, the relative rotation over the time. In RBS-joints, the elongation and shortening of the reduced beam section at upper and lower beam flange was measured, in order to compute the local curvature of the dissipative zone (Figure 7b). Finally, for the specimens with LS-joints structural damage was expected to concentrate on the end-plates. Two displacement transducers were applied at top beam flange and respectively at bottom flange. As shown in Figure 7c for the joint 1a, RD1a**C**T measured the total response of the end-plate and beam, whereas RD1a**B**T recorded the response of the beam. The bending of the end-plate can be computed by subtracting the quantity RD1a**B**T from RD1a**C**T. Based on numerical simulations, column web panels in all cases do not present ine-

lastic response, as they were strengthened from both sides sufficiently. Therefore, their response was not measured separately.

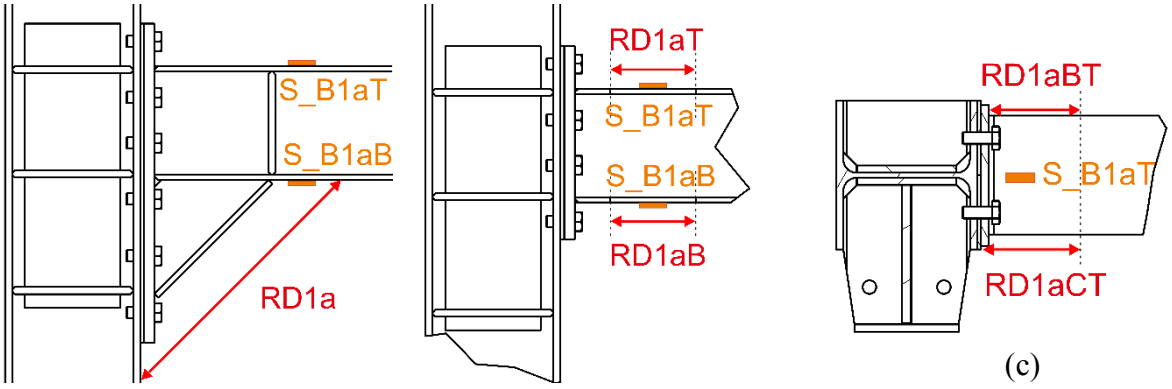

Figure 7: Local instrumentation scheme at Joint 1a (1st floor, axis A, beam start) (a) haunched joint, (b) reduced beam section joint, (c) low seismicity joint.

	ICP	MEMS (high resolution)	MEMS
Meas. Range (g)	± 0.5	± 3	± 2
Freq. Range (Hz)	0.15-1000	0-500	0-1000
Sensitivity (mV/g)	10000	900	600
Resolution (g)	0.000008	0.000022	0.001581
Noise (µg/√Hz)	0.32	1	50
Resolution (g)	0.000008	0.000022	C53
Number of sensors	4	2	8
Channels	1	2	2
Label in instr. Scheme	Acc1-Acc4	M-HR1xy & M-HR2xy	M1xy – M6xy
Main Target	System Identification (ambient measurements)	System identification and seismic response	Seismic response
Number of sensors	4	2	6

Table 2: Properties of accelerometers.

3 NUMERICAL INVESTIGATION

Structural models of the specimens were developed in SAP2000 [19]. In order to implement the initial stiffness of connections, as well as their non-linear response detailed pre-test Finite Element Analyses (FEA) were performed on the beam-to-column joints and the column base, using Abaqus v.2021 [20].

3.1 Detailing

For the joint sub-models, the beam and column lengths, shown in Figure 8, were adapted such that the inflexion points of the test structure corresponded to the beam and column ends of the model. FEA models in Abaqus consisted of solid linear hexahedral elements of type C3D8R. Regarding the elastic material properties of steel, Modulus of Elasticity (E = 210000 N/mm^2), density (7,850·10^{-9} tons/mm^3) and Poisson's ratio (v = 0.3) were considered. Expected material properties were inserted for the analyses (see Figure 9) from the literature

[21][22]. Beams, end-plates and haunches were assigned S235, while columns S355. Material hardening and cyclic-response was assumed in this case as isotropic (load introduction was monotonic). The engineering stress-strain curves were computed into true stress - true strain curves according to Eqs. D.1 and D.2 from EN 1993-1-5 [23]. The material model for the bolts was based on [22]. Concerning the interactions, "tie constrain" was applied for the welded connections and "contact interaction" was used for all surfaces in contact. For the normal contact behavior was chosen "hard contact" allowing separation. The friction coefficient for tangential behavior was set 0.3. Regarding the discretization method, the mesh was adapted to the demand of different components emphasizing on areas, where plastic strains were expected. A sensitivity analysis was performed and mesh growth was optimized until the results were independent from the mesh size. The loading was introduced as incrementally increasing horizontal displacement up to 100 mm at the tip of the column (RP-2) using a smooth step function. A pinned support was arranged at column base (RP-1) and a mobile support at beam end (RP-3). The selected analysis type was "Dynamic Explicit". Time and mass scaling were arranged properly that inertia contributions do not influence the results. Geometrical non-linearities were also considered.

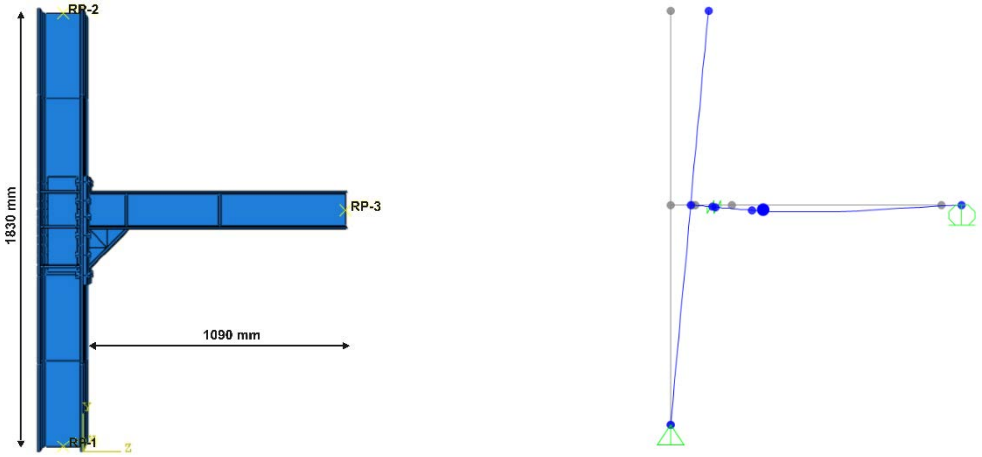

(a) (b)

Figure 8: Finite Element Models; (a)Model in Abaqus for the haunched joint, (b) Model in SAP2000v21.

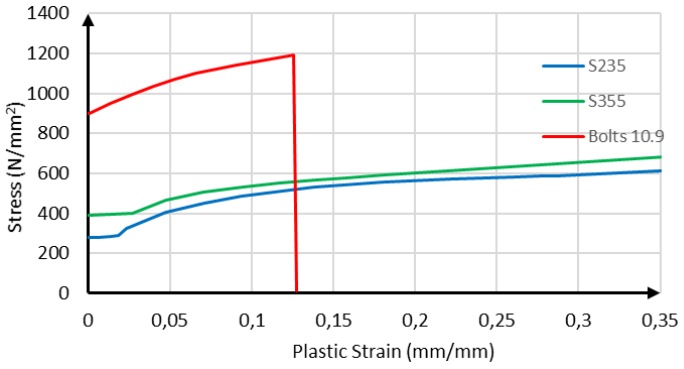

Figure 9: Material Properties: true stress-true strain for S355 (column), S235 (beams) and bolts 10.9.

Subsystem models with the same geometry were also developed in SAP2000 (Figure 8b). The haunch and the reduced beam section were modelled by using non-prismatic cross-sections with variable cross-sectional depth and width respectively. The strengthening of column panel was implemented through the panel zone command of SAP2000, defining the corresponding plate thickness. In addition, a rotational spring was arranged at beam end to

consider for the connection flexibility. Plastic Hinges (PH) were used to simulate the non-linear response of the corresponding dissipative zones. Springs and plastic hinges properties were validated based on the numerical results of FEA from Abaqus, as shown in Figure 10 and outlined in Table 3. The position of the plastic hinges was indicated by the plastic strain distribution, as illustrated in Figure 11. The kinematic hysteresis type was selected for the plastic hinges. The moment-rotation curves of the investigated joints were plotted in Figure 12a. Bending moment was calculated for column flange for all configurations.

	Haunched	RBS	LSJ
Spring Stiffness (kNm/rad)	20000	7450	4000
Yield Moment (PH) (kNm)	35	23	22.5
Yield Rotation (mrad)	8	7.5	9.5
Strain hardening	1.20	1.40	1.85
Distance PH from beam start (mm)	200	110	10

Table 3: Properties of rotational springs and plastic hinges.

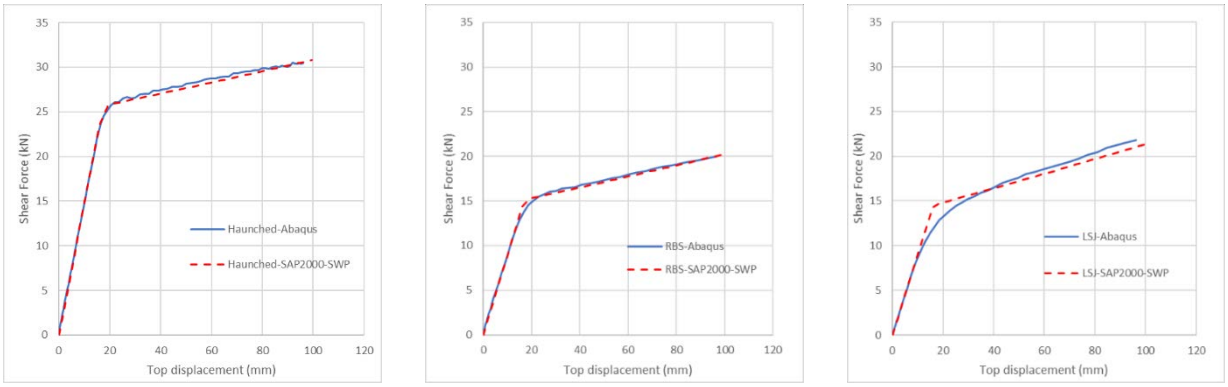

(a) (b) (c)

Figure 10: Pushover result Abaqus vs. SAP2000 (a) haunched joint, (b) reduced beam section joint, (c) low seismicity joint.

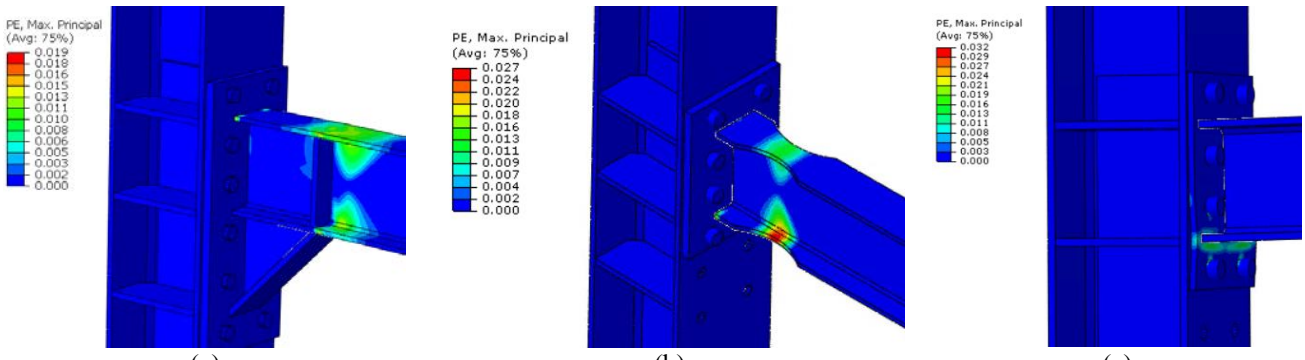

(a) (b) (c)

Figure 11: Plastic strain distribution for rotation 25 mrads; (a) haunched joint, (b) reduced beam section joint, (c) low seismicity joint.

Apart from beam-to-column joints, particular attention was devoted to column base connections. On the one hand, it was desired that structural damage concentrates on the beam ends. On the other hand, this had to be achieved considering the capacity of the available

shaking table. Because of laboratory height limits, pinned support with clevis pins as in [16] could not be used. Therefore, the solution illustrated in Figure 12b was developed to approach pinned boundary conditions. The numerical simulation showed that the connections' stiffness decreased significantly, but it was not completely pinned. Its rotational stiffness was considered in global model using a spring with rotational stiffness of 450kNm/rad.

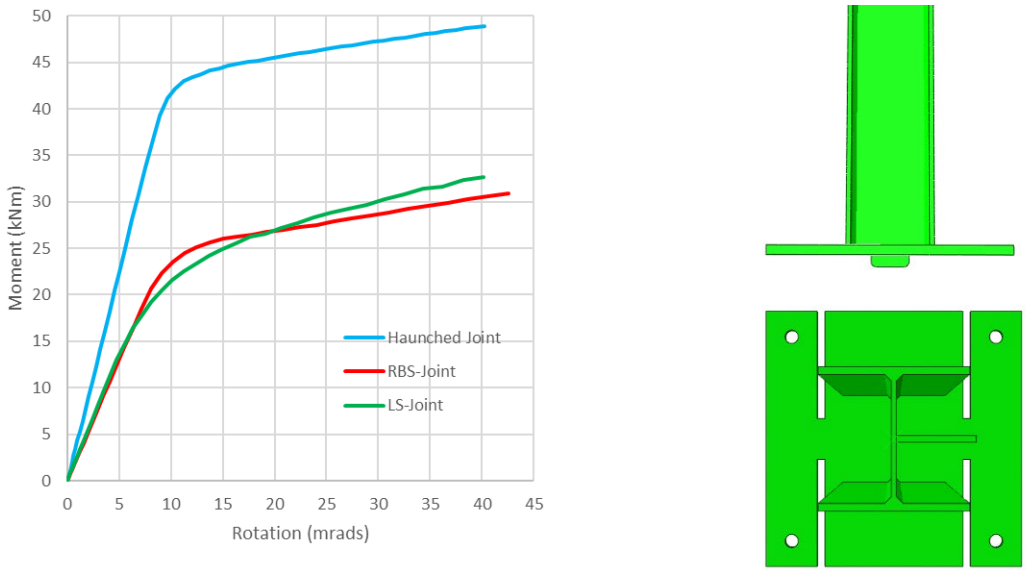

(a) (b)

Figure 12: (a) Moment-rotation curves of beam-to-column joints (Abaqus models), (b) column base connection.

3.2 Global Models

Global models developed in SAP2000v21 consider the space framed specimens as 3D-models. In the MRF-direction, the beam-to-column joint properties, namely rotational stiffness and non-linear response, were implemented through springs and plastic hinges validated on solid FEA results. All secondary beams (HEA140) were modelled as pinned connected to both ends. The braces in transverse direction (hollow sections Q50·5) were considered as pinned as well. The pressure vessel was supported on 4 steel C-Profiles. Their real cross-section was modelled in Section Designer. The main body of the vessel was simulated by a cantilever column with a pipe cross section (radius equal to containers middle radius (r = 700 mm) and thickness equal to real thickness t = 2 mm). At a height of 2/3 of the total height, its mass was assigned as lumped mass. The I-Profiles, which were used only as dead load for the structure were modelled as nodal loads at the corresponding secondary beams. Models with and without diagonal bracings substituting a diaphragm were computed. All results presented in this paper consider them as existing. Finally, plastic hinges were assigned to all column ends. Plastic rotation angle was calculated according to the following formula:

$$\theta_y = \frac{M_p \cdot L_c}{6 \cdot E \cdot I_c} \cdot \left(1 - \frac{N}{N_p}\right) \quad (1)$$

where M_p is plastic bending strength of column, L_c the length of column, E the modulus of elasticity, I_c the column's moment of inertia around the strong axis, N is the normal force in column and N_p the plastic axial strength of column.

Modal analysis and static non-linear (pushover) analysis were carried out for the three specimens. Modal properties, as outlined in Table 4, will act as the main criterion to update

the models after the erection of the specimens on the shaking table and before the tests, considering on the experimental dynamic identification under white noise excitation of low amplitude. Capacity curves (see Figure 13) resulted from the non-linear static analysis indicate the sequence of the plastic mechanisms. After a horizontal top displacement of approximately 55 mm, all three specimens tend to behave inelastic, with increasing plastic strains in the corresponding dissipative zone. No structural damage was indicated at the columns, as they remained elastic even for top displacements up to 200 mm.

	SP1-HJ	SP2-RBS	SP3-LSJ
Period T_1 (s) MRF- Direction	0.323	0.390	0.393
Period T_2 (s) BF- Direction	0.085	0.084	0.085
Period T_3 (s) – torsional mode	0.072	0.072	0.074
Period T_4 (s) – MRF-Direction	0.065	0.069	0.070

Table 4: Modal Properties of global models.

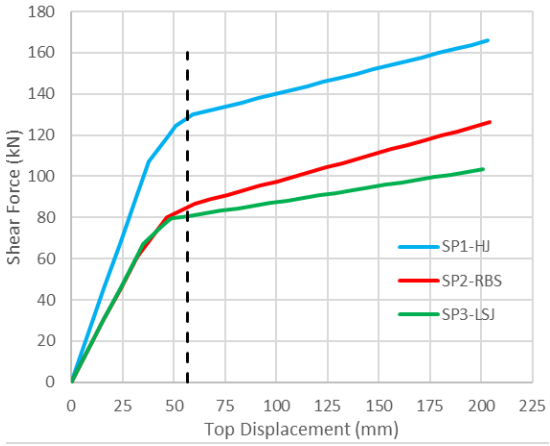

Figure 13: Capacity curves for the three frame specimens.

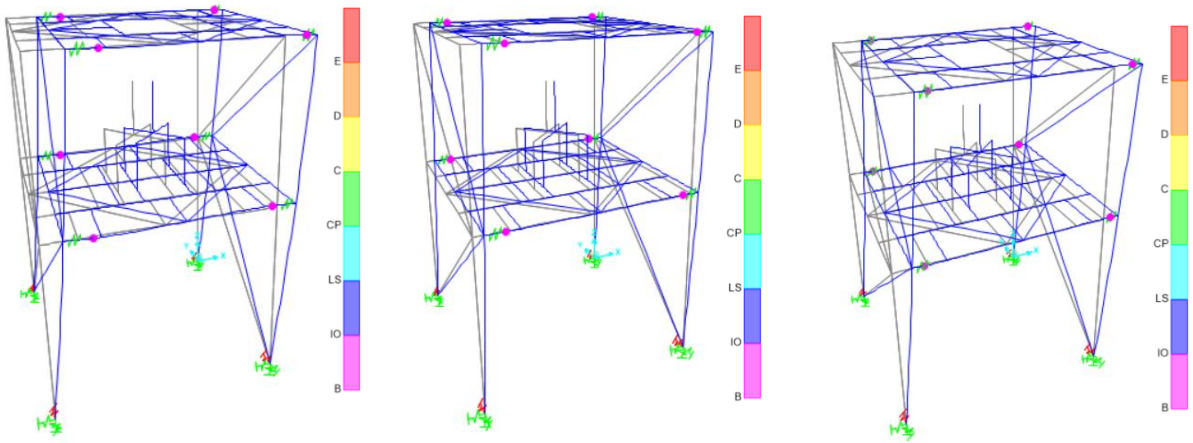

Figure 14: Damage state for roof displacement 1.5% (55 mm); (a) SP1-HJ, (b) SP2-RBS, (c) SP3-LSJ.

4 EARTHQUAKE SCENARIOS

After identifying the main structural properties, different real and artificial response-history analyses were carried out to investigate the structural integrity of the frame specimens and determine the dataset of possible accelerograms for the experimental tests. For the sake of clarity, the results of response history analyses using a real accelerogram with Peak Ground Acceleration (PGA) or a_g = 0.408g, illustrated in Figure 15a, scaled at three intensity levels of 0.3g, 0.4g and 0.6g are outlined below. PGA was used as a demand parameter for the scaling of the record. The selected record provided an amplification at the frequency range of the fundamental period of the specimens (0.3-0.4s), as shown in Figure 15b.

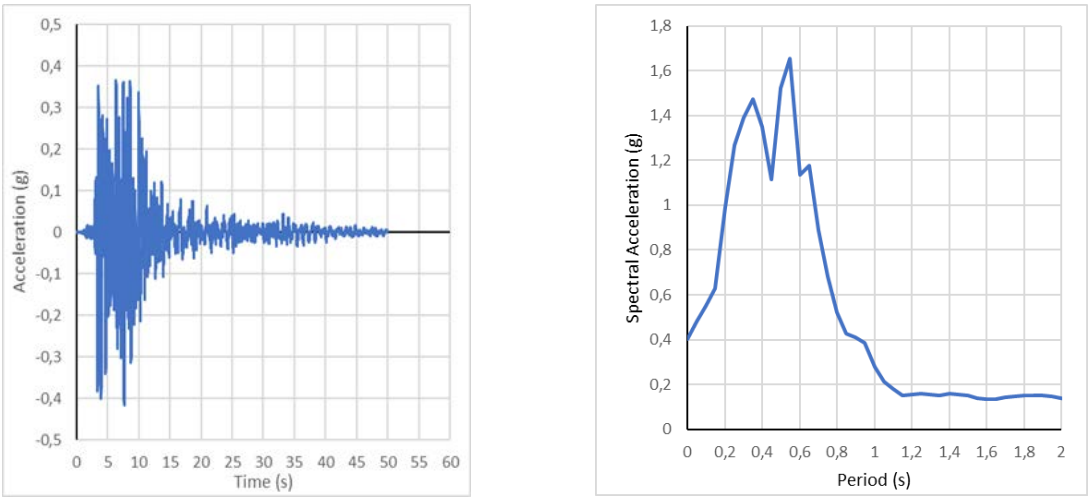

(a) (b)

Figure 15: Recorded input motion (Lefkada 14/08/2003); (a) Time history, (b) Spectral Acceleration.

The analyses of this record have shown, that for a_g = 0.3g only SP3-LSJ, slightly left the elastic range (Figure 16c), for a_g = 0.4g the joints of SP2-RBS and SP3-LSJ exhibited limited plastic rotation up to 3 mrads and SP1-HJ remained elastic. However, for a_g = 0.6g all specimens behaved non-linear with maximum plastic rotation at joints between 4.5 to 8 mrads. Horizontal Roof Displacement (HRD) over the time was plotted for the maximum investigated intensity for all specimens in Figure 17. Both maximum HRD, compared with the capacity curves (Figure 13), as well as the residual HRD, indicated the presence of slight damage for the highest investigated level of intensity. Supplementary to the above-mentioned information, Peak Floor Acceleration (PFA) for each floor of the structure and Maximum Inter-story Drift Ratio (IDR) are summarized in Table 5. The gradual decrease of the acceleration amplification over the structure height (ratio PFA/PGA) with increasing PGA was also considered as an indicator, that confirmed the existence of (limited) structural damage. Values of IDR higher than 1.2, which were observed for all specimens for intensity a_g = 0.6g and for SP2-RBS and SP2-LSJ for a_g = 0.4g, categorized specimens regarding the expected damage, according to HAZUS [24], as moderate damaged.

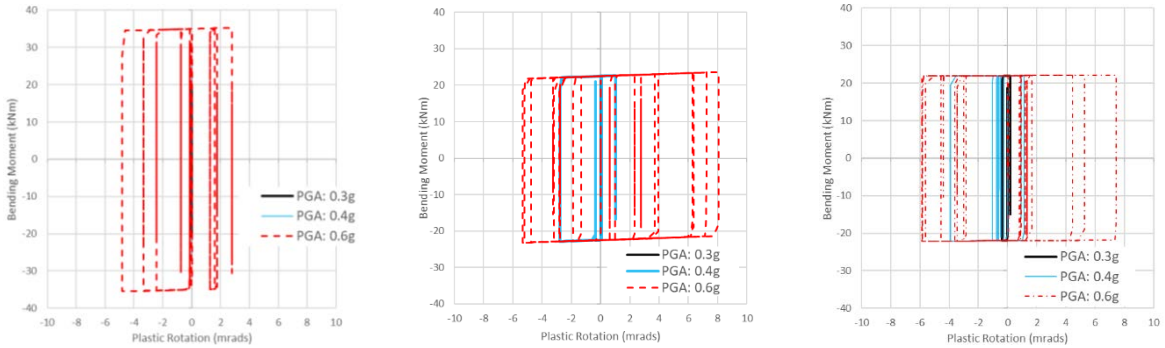

(a) (b) (c)

Figure 16: Response of plastic hinge at 1st floor; (a) SP1-HJ, (b) SP2-RBS, (c) SP3-LSJ.

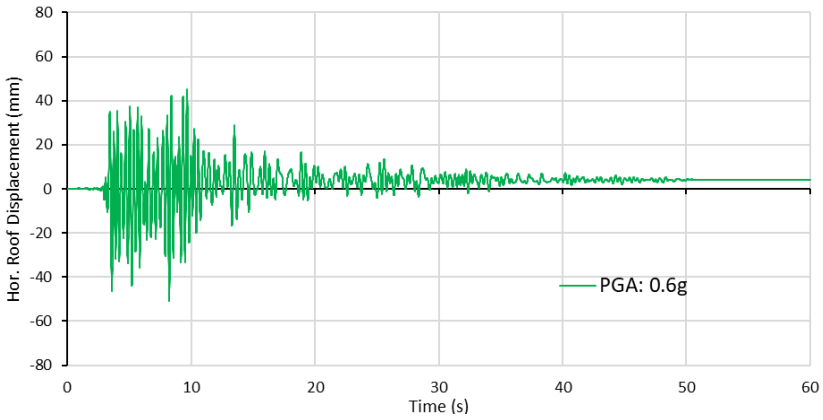

(a)

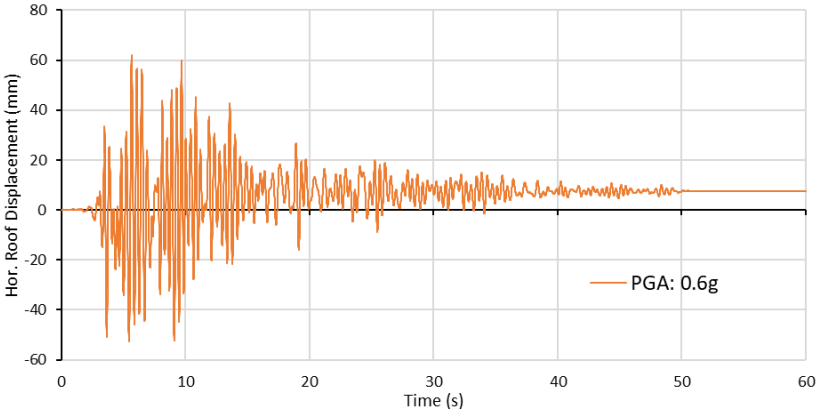

(b)

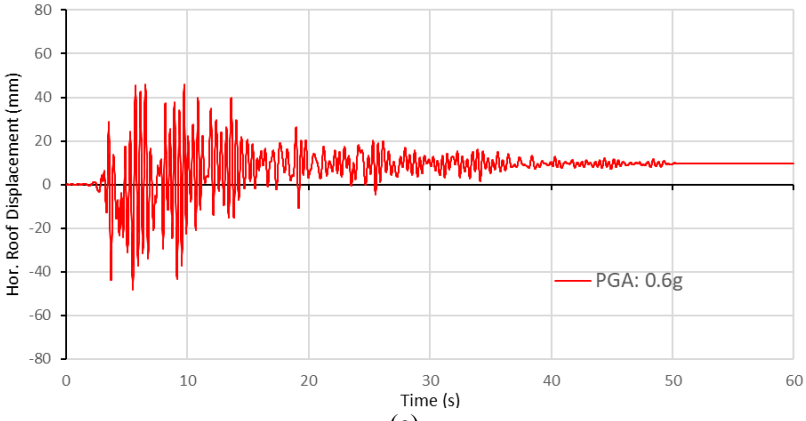

(c)

Figure 17: Response history of horizontal roof displacement; (a) SP1-HJ, (b) SP2-RBS, (c) SP3-LSJ.

	SP1-HJ			SP2-RBS			SP3-LSJ		
PGA (g)	*0.3*	*0.4*	*0.6*	*0.3*	*0.4*	*0.6*	*0.3*	*0.4*	*0.6*
1st PFA (g)	0.53	0.71	0.83	0.56	0.65	0.80	0.54	0.61	0.76
2nd PFA (g)	0.83	1.11	1.21	0.88	1.06	1.19	0.85	0.97	1.08
max. HRD (mm)	21.9	29.2	51.2	33.5	44.4	62.2	32.6	44.6	56.5
res. HRD (mm)	0.00	0.84	4.14	0.08	1.27	7.61	0.20	1.11	11.31
max. IDR (%)	0.7	0.97	1.58	1.01	1.32	1.81	0.99	1.31	1.65

Table 5: Response-history analysis results.

5 DAMAGE SENSITIVE INDICATORS

The damage assessment concept developed within the Robust project includes mainly three steps. First of all, the comparison of damage sensitive factors of the reference state (undamaged – healthy state) before a seismic event and the investigated state (possibly damaged state) after the end of a seismic event. Apart from the common system identification in terms of frequencies, modal shapes and damping ratios, transmissibility-based features, as elaborated in [25] will be investigated during the tests and implemented in the damage detection tool. The Transmissibility Assurance Criterion (TAC), which is based on the cross-spectral density between two points, whose response is recorded by accelerometers, as indicated in [13], can be used to evaluate the fitting degree between healthy and investigated (possibly damaged) state in a predefined frequency range. As long as the system remains elastic, they present a strong fitting, whereas in occurrence of damage the deviation increases. Those measurements are conducted under ambient excitation and can be evaluated using Operational Modal Analysis methods [26]. Ambient excitation will be substituted within the experimental program by low amplitude noise excitation of the shaking table prior and after each test. Furthermore, the response of the structure during the earthquake (strong motion) is considered. Within this context, maximum and Root Mean Square (RMS) measured values are compared with precalculated analyses of similar seismic scenarios from a database. The similarity criteria are defined based mainly on the elastic spectrum acquired from the accelerometer located on the foundation/shaking table. Moreover, sequent segments of the structure response prior and after ground motion peaks are investigated to identify differences between them. Finally, the conclusions of the vibration-based damage detection are compared with the expected damages based on vulnerability analyses. During the tests, the global instrumentation system supports the vibration-based damage detection, whereas the local monitoring system is used to label the existence of damage. The main damage-sensitive indicators (DSI) for both ambient and seismic excitation are listed in Table 6.

DSI	Domain	Notes	Excitation
RMS	Time	RMS_x / RMS_f floor response normalized to input acceleration measured on foundation	Seismic & Ambient
Drift Estimator	Time	Double integration of acceleration including filtering and detrending	Seismic
Accel. Amplification	Time	PFA_i/PGA or PFA_i/PFA_j	Seismic

		ratio of peak floor accelation of different floor or floor over foundation	
Frequency Estimators	Frequency	f_i	Ambient
Modal Shapes	Frequency	Mainly φ_1 and φ_4 (modal shapes in MRF direction)	
Modal Damping Ratio	Frequency	ζ_i	Seismic & Ambient
$TAC_{a,b}$	Frequency	TAC can be evaluated for all combinations of sensors	Seismic (segmented) & Ambient

Table 6: List of damage sensitive indicators for vibration-based damage detection.

6 CONCLUSIONS

In the framework of the German funded research project "ROBUST", shaking table tests were designed – for investigating a scaled structure (i.e. related to a monitored industrial facility). As the shaking table tests are currently in the final preparation phase (i.e. structural elements have been fabricated and delivered, respectively the first frame specimen is being assembled on the shaking table) within the current paper – an outline was presented with regard to the experimental program and the pre-test numerical investigations.

The designed frame specimens comprised a compromise between a scaled mock-up of the monitored industrial facility and the boundary conditions of the available shaking table. From the point of view of adopted material, S235 structural steel was selected for the dissipative members of the primary structure, whereas S355 for the non-dissipative elements (e.g. columns). The numerical investigations have shown that slight-to-moderate damage can be achieved, especially for SP2-RBS and SP3-LSJ. After the erection of the frame specimens, their modal properties will be identified and the real or artificial accelerogram will be selected properly to increase the possibility of damage occurrence (i.e. seismic energy dissipation through development of plastic hinges). The above-described numerical analyses were carried out based on material properties from conducted tests. For S235, a yield stress of 279 N/mm^2 was considered. However, it cannot be excluded that the real material will be characterised by a higher overstrength. Regarding SP2-RBS and SP3-LSJ, the target is to identify damage at the primary structure, whereas the SP1-HJ will be used at the second phase of the experimental campaign to investigate the response of non-structural element attached on it. Concerning, the detailed numerical analysis of the beam-to-column joints, it was proven that the both the initial stiffness and the non-linear response can be sufficiently implemented in global models using springs and plastic hinges, although in the case of LSJ, as plastic strain concentrated on the end-plate, the fitting between SAP2000 and Abaqus presented a higher deviation, overestimating slightly the yield point. Regarding the global structural models, non-linear static analyses and dynamic response history analyses were in good agreement. The maximum horizontal roof displacement for an intensity of 0.6g was close to the threshold value of 55 mm defined on the capacity curves to label damage existence.

ACKNOWLEDGEMENTS

The results presented in the current paper were obtained within the project, "*ROBUST – User-oriented early warning system based on smart sensor networks and digital building models. Development- Installation and Application of sensor-based monitoring systems with integration in BIM-Real-Time Damage Detection in critical facilities* ", which is carried out in

the framework of the industrial collective research program. The project is financially supported by the German Federal Ministry of Education and Research. The support is hereby gratefully acknowledged.

REFERENCES

[1] G. Balaskas, B. Hoffmeister, C. Butenweg, M. Pilz, A. Bauer, Earthquake Early Warning and rapid response system based on smart seismic and monitoring sensors embedded in a communication platform and coupled with BIM models. M. Papadrakakis, A. M. Fragiadakis eds. *8th ECCOMAS Thematic Conference on Computational Methods in Structural Dynamics and Earthquake Engineering,* Streamed from Athens, Greece, June 27-30, 2021.

[2] O. S. Salawu, Detection of structural damage through changes in frequency: A review. Eng. Struct. 19(9),718-23, 1997.

[3] E. P. Carden, P. Fanning, Vibration based condition monitoring: A review, Structural Health Monitoring, 3(4), 355-77, 2004.

[4] G. Herna, R. Testa Modal Analysis for damage detection in structures. Journal of Structural Engineering, 117(10), 3042-63, 1991.

[5] F. Vidal, M, Navarro, C. Aranda, T. Enomoto, Changes in dynamic characteristics of Lorca RC buildings from pre- and post-earthquake ambient vibration data, Bulletin of Earthquake Engineering, 12(5), 2095-110, 2014.

[6] F. Lorenzoni, M. Caldon, F. da Porto, C. Modena, T. Aoki, Post-earthquake controls and damage detection through structural health monitoring. Applications in l'Aquilla, Journal Civil Structural Health Monitoring, 8(2), 217-36, 2018.

[7] A. Pandey, M. Biswas, M. Samman, Damage detection from changes in curvature mode shape, Journal of Sound and Vibration, 145(2), 321-332, 1991.

[8] Y. Reuland, P. Lestuzzi, I. Smith, Measurement-based support for post-earthquake assessment of buildings, Journal of Structural Infrastructure Engineering,15(5), 647-62, 2019.

[9] S. Atamturktur, T. Li, M. Ramage, I. Farapour, Load carrying capacity assessment of a scaled masonry dome: Simulations validated with non-destructive and destructive measurement, Construction Building Materials, 34, 418-29, 2012.

[10] A. Kita, N. Cavalagli, M. Masciotta, P. Lourenco, F. Ubertini, Rapid post-earthquake damage localization and quantification in masonry structures through multidimensional non-linear seismic IDA,Journal of Engineering Structures, 219, 110841, 2020.

[11] S.-H Hwang, D. Lignos, Assessment of structural damage detection methods for steel structures using full-scale experimental data and nonlinear analysis, *Bulletin of Earthquake Engineering* 16 (7), pp. 2971–2999, 2018.

[12] O. Anci, O.Abdeljaber, S. Kiranyaz, M. Hussein, M. Gabbouj, D. Inman, A review of vibration-based damae detection in civil structures: From traditional method to macine learning and deep learning applications, Mechanical Systems and Signal Processing, 147, 107077, 2021.

[13] P. Martakis, Y. Reuland, A. Stavridis, E. Chatzi, Fusing damage-sensitive features and domain adaptation towards robust damage classification in real buildings, Journal of Soil Dynamics and Earthquake Engineering, 166, 107739, 2023.

[14] Y. Reuland, P. Martakis, E. Chatzi, A Comparative Study of Damage-Sensitive Features for Rapid Data-Driven Seismic Structural Health Monitoring, Appl. Sci.,13,2708, 2023.

[15] prEN 1998-1-2:2021 (2022) Eurocode 8: Design of structures for earthquake resistance - Part 1-2: Earthquake resistance design of structures, CEN European Committee for Standardisation, Brussels, Belgium (version: 28.02.2022).

[16] R. Don, G. Balaskas, C. Vulcu, B. Hoffmeister, Steel and composite joints with Dissipative Connection for MRFs in Moderate Seismicity: Experimental and Numerical Programs, Ernst & Sohn, Steel Construction 16 (2023), Article: 202200044, 2023.

[17] R. Don, G. Balaskas, C. Vulcu, B. Hoffmeister, Steel and composite joints for MRFs in moderate seismicity: experimental and numerical program, Ernst & Sohn, Special issue: SDSS 2022 5, Issue 4, S. 857-866, 2022.

[18] National Instruments, Specification Compact-RIO 9045.

[19] CSI Berkley, SAP2000 v24, Copyright Computers and Structures, 2022.

[20] Dassault Systemes, SIMULIA Abaqus FEA (software), 2021.

[21] R. Don, A. Ciutina, C. Vulcu, A. Stratan, Seismic resistant slim floor bem to column joints: experimental and numerical investigations, *Steel and Composite Structures*, 37 (3), pp. 307–321, 2020.

[22] C. Vulcu, D. Dubina, Seismic protection of structures using a hybrid system: Buckling restrained brace and magneto rheological damper, M. Papadrakakis, A. M. Fragiadakis eds. *7th ECCOMAS Thematic Conference on Computational Methods in Structural Dynamics and Earthquake Engineering,* Rhodes, Greece, June 15-17, 2017.

[23] EN 1993-1-5:2006 Eurocode 3: Design of steel strctures – Part 1-5: Plated structural elements. Brussels, Belgium: CEN European Committee for Standardisation.

[24] FEMA – NIBS, Multi-Hazard Loss Estimation Methodology, HAZUS Earthquake Model Technical Manual 4.2 SP3, Federal Emergency Management Agency, Washington D.C., 2020.

[25] Y.-L. Zhou, H. Cao, Q. Liu, M.A. Wahab, Output-based structural damage detection by using correlation analysis together with transmissibility, Journal of Material, 10(8), 2017.

[26] C. Rainieri, G. Fabbrocino, Operational Modal Analysis of Civil Engineering Structures. An introduction and Guide for Applications, 1st ed. New York, Springler NY, 2014.